Hindawi
Advances in Civil Engineering
Volume 2019, Article ID 5952319, 16 pages
https://doi.org/10.1155/2019/5952319

Research Article

Parametric Push-Out Analysis on Perfobond Rib with Headed Stud Mixed Shear Connector

Shuangjie Zheng,[1] **Chen Zhao**,[2] **and Yangqing Liu**[3]

[1]*College of Civil Engineering, Huaqiao University, Xiamen 361021, China*
[2]*Shanghai Municipal Engineering Design Institute (Group) Co. Ltd., Shanghai 200092, China*
[3]*Department of Bridge Engineering, Tongji University, Shanghai 200092, China*

Correspondence should be addressed to Shuangjie Zheng; sjzheng@hqu.edu.cn

Received 25 November 2018; Revised 15 February 2019; Accepted 20 February 2019; Published 18 March 2019

Academic Editor: Giovanni Minafò

In steel and concrete composite structures, it is unfavourable to install many headed studs or perfobond ribs with narrow spacings at the joints. To solve this problem, a new type of a mixed shear connector was developed by combining a headed stud and perfobond rib at the same steel beam flange. In this paper, totally nine push-out tests were conducted. The main purpose was to compare the failure mode and the load-slip behavior of the headed stud, perfobond rib, and mixed shear connector. Furthermore, 19 nonlinear finite element simulations were performed. The effects of connector dimension and material properties on the structural behaviors of mixed shear connectors were studied. Based on the experimental and parametric study, an analytical equation was finally proposed to evaluate the shear capacity of perfobond rib with a headed stud mixed shear connector.

1. Introduction

In the past few decades, composite structures made of steel and concrete have been increasingly used in construction and bridge engineering. The main reason is their optimum structural performance and favourable cost. To achieve the load transfer between steel and concrete components, various types of shear connectors have been proposed, such as headed studs [1], perfobond ribs [2–4], channel connectors [5], bolted connectors [6], and composite dowels [7]. The headed stud connector is most popular in engineering practice. The longitudinal shear is resisted by a stud shank, and the uplift separation is prevented with an anchorage head. However, the headed stud has some disadvantages, such as the requirement for specific welding equipment and the fatigue problem under cyclic loading [8, 9].

To ease the installation and to improve the fatigue performance of shear connectors, an alternative connector named perfobond rib connector was developed by a German design company in the 1980s. The perfobond rib connector consists of a flat steel plate with several holes. Concrete dowels will form in these holes after casting to resist both shear and uplift forces. The perfobond rib connector has some advantages over the headed stud, such as easier installation by using continuous fillet welds, higher shear stiffness, and favourable fatigue performance. Thus, the perfobond connectors are increasingly designed and used in composite structures [10, 11].

Recently, extensive research has been done to reveal the structural behavior of headed stud and perfobond rib shear connectors [12–16]. The effects of the shank diameter, stud length, material properties, and loading directions on the shear behavior of the headed stud have been studied [12, 13]. The effects of the hole number, hole diameter, configuration of the rebar in the hole, dimension of the perfobond rib, and material properties on the shear behavior of the perfobond rib have been investigated [14–16]. According to these investigations, the shear capacity of shear connectors can be conveniently increased by using more headed studs or perfobond ribs. However, installing many headed studs or perfobond ribs at one steel beam flange would narrow the spacings, which is unfavourable for the bearing performance of shear connectors. It would also increase the difficulty in placing the reinforcing bars between headed studs and perfobond ribs.

In this paper, a new type of mixed shear connector was developed, combining headed stud and perfobond rib at the same steel beam flange. A total of nine push-out specimens were designed and tested. The main purpose was to compare the shear capacity and the load-slip behavior of the headed stud, perfobond rib, and mixed shear connector. Moreover, nonlinear finite element models were generated to study further the structural behaviors of mixed shear connectors concerning the connector dimension and material properties. Based on the experimental and numerical results, an analytical equation was derived to predict the shear capacity of perfobond rib with headed stud mixed shear connector.

2. Push-Out Test

To confirm the reliability of the push-out analysis for a perfobond rib with a headed stud mixed shear connector, nine push-out tests were introduced. As shown in Table 1, these tests could be equally divided into three groups in terms of the connector type. The groups HS and PR were the specimens installed with the headed studs and perfobond ribs, respectively. The group MS was the specimen of the perfobond rib with the headed stud mixed shear connector which was installed with four headed studs and one perfobond rib at each steel flange. The variables of the headed stud were the stud shank diameter d_s and the stud length l_s. The parameters of the perfobond rib were the hole diameter d_p and the rebar diameter d_r. The yield strength and ultimate strength of the stud, the rebar, and the structural steel were obtained from tension tests and denoted as f_{sy}, f_{ry}, f_y and f_{su}, f_{ru}, f_u, respectively.

The layout of the push-out test specimens is shown in Figure 1. Apart from the connector type, all the test specimens were identical in terms of the dimensions. Each specimen comprised one steel H-beam and two concrete slabs. The headed stud or perfobond rib was welded to the steel beam flange. A perforating rebar was installed in the hole of the perfobond rib. The bond was prevented by greasing the contact surfaces before concrete casting. Styrofoam was attached to the bottom of the perfobond rib to eliminate the bearing stress.

As shown in Figure 2, the specimens were tested by using a hydraulic loading machine. The shear force between steel and concrete was applied by pushing down the steel H-beam. Four displacement gauges were installed at the level of the headed stud or the hole of the perfobond rib to measure the relative slip. The applied load and relative slips were both automatically and continuously recorded. Therefore, the push-out failure and load-slip curves of shear connectors could be obtained to verify the proposed finite element model.

3. Finite Element Analysis

3.1. General. The finite element model of a typical push-out test was established with only one half of the specimen in order to save the analysis time, as shown in Figure 3. One purpose of this analysis was to investigate the inner failure by using validated finite element models instead of expensive and time-consuming push-out tests. Another purpose was to find out how these finite element models could support the deduction of design rules for the perfobond rib with the headed stud mixed shear connector. To assign the modelling strategy to other connector types, the general analysis package ABAQUS [17] was adopted to simulate the push-out tests of the mixed shear connector. The dynamic explicit method was used to consider both material and geometric nonlinearities [18–22]. The loading rate was carefully concerned by comparison with the push-out test results and finally taken as 0.1 mm/s to assure the quasi-static loading process. The kinetic energy was controlled within 5% to 10% of the total internal energy. A semiautomatic mass scaling method was used with the target time increment of 0.002 s to achieve a balance between solution time and accuracy.

3.2. Finite Element Type and Mesh. As shown in Figure 3, a typical push-out test was modelled with the relevant support constraints in the symmetry layers. Discrete rigid elements (R3D4) were introduced to mesh the jacking header and the base plate. Eight-node reduced integration elements (C3D8R) were chosen to simulate the concrete slab, steel beam, headed stud, perfobond rib, and perforating rebar. Three-dimensional two-node truss elements (T3D2) were used to model the other rebars. A global coarse mesh was applied to save analysis time using an overall size of 10 mm. In order to achieve more accurate results, a locally refined mesh with a smallest size of about 5 mm was applied at the region of the headed stud and perfobond rib.

3.3. Interaction and Boundary Conditions. The boundary condition (BC), as shown in Figure 4, was applied to the symmetric planes of the model. The reference point of the base plate was fixed in all directions. A downward enforced displacement of 10 mm was applied to the reference point of the jacking header which represented the action of the hydraulic loading machine. Shear forces were induced at the interface of the shear connectors and the concrete slab. The perforating rebar was tied to the surrounding concrete, while the other rebars were embedded inside the concrete slab. Contact interactions were applied at the interfaces of the jacking header to steel beam, concrete slab to base plate, steel beam to concrete slab, and concrete slab to shear connectors. General contact interactions were applied by matching predefined master and slave surface pairs [17]. A "hard" contact was used in the normal direction to prevent penetration. The contact pressure could be transmitted, and possible separation was allowed when the pressure was zero or negative. The tangential behavior was defined by penalty frictional formulation. After trial calculations, the favourable frictional coefficient was taken as 0.5 for the contact between the base plate and concrete slab, while the other contact interactions were assumed to be frictionless.

3.4. Material Modelling of Concrete. As shown in Figure 5, the nonlinear behavior of the concrete material in

Table 1: Push-out test specimens.

Group	Headed stud				Perfobond rib				Steel		Concrete
	d_s (mm)	l_s (mm)	f_{sy} (MPa)	f_{su} (MPa)	d_p (mm)	d_r (mm)	f_{ry} (MPa)	f_{ru} (MPa)	f_y (MPa)	f_u (MPa)	f_{cu} (MPa)
HS	22	200	370	465	—	—	—	—	410	545	70.3
PR	—	—	—	—	60	20	382	547	410	545	70.3
MS	22	200	370	465	60	20	382	547	410	545	70.3

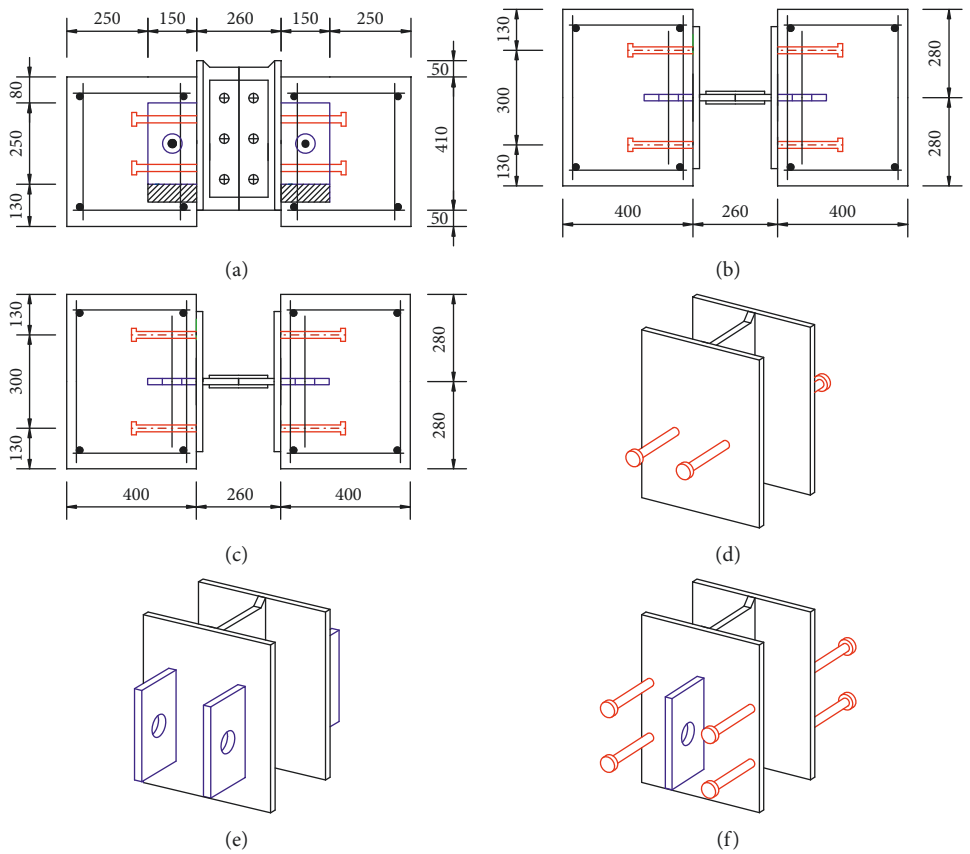

Figure 1: Layout of the push-out test specimen. (a) Front view. (b) Top view. (c) Side view. (d) Headed stud connector. (e) Perfobond rib connector. (f) Mixed shear connector.

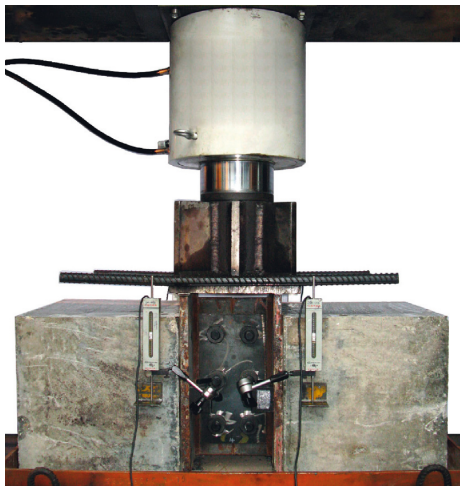

Figure 2: Test setup and instrumentation.

compression and tension was presented by a uniaxial compressive stress-strain curve and a tensile stress-crack width relationship, respectively.

The concrete material constitutions in compression were governed by equation (1) [23, 24]. As shown in Figure 5(a), the first part of the stress-strain curve is assumed to be elastic. The following two parts are a nonlinear parabolic portion and a descending branch, respectively:

$$\sigma_c = \begin{cases} E_c \varepsilon_c, & 0 \le \varepsilon_c \le 0.4 f_c / E_c, \\ \dfrac{k \cdot \eta - \eta^2}{1 + (k-2) \cdot \eta} f_c, & 0.4 f_c / E_c < \varepsilon_c \le \varepsilon_{cp}, \\ \left(1 - 0.15 \dfrac{\varepsilon - \varepsilon_{cp}}{\varepsilon_{cu} - \varepsilon_{cp}}\right) f_c, & \varepsilon_{cp} < \varepsilon_c \le \varepsilon_{cu}, \end{cases} \quad (1)$$

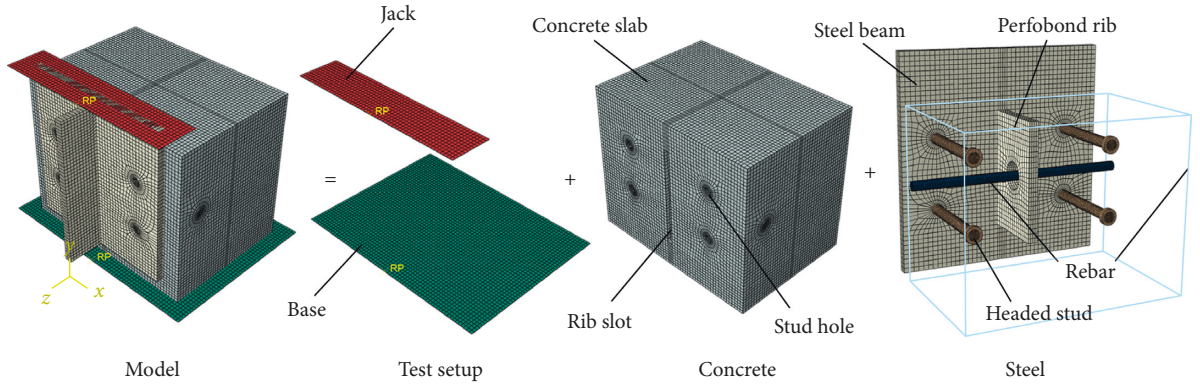

Figure 3: Finite element model.

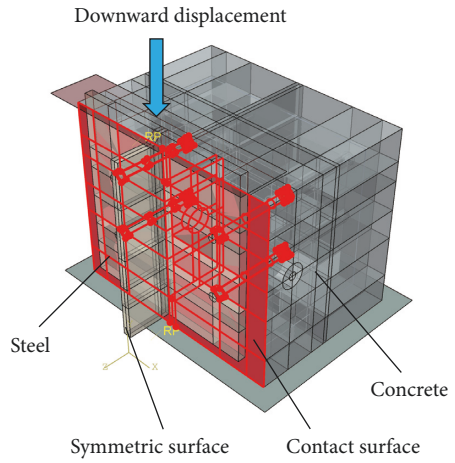

Figure 4: Interaction and boundary conditions.

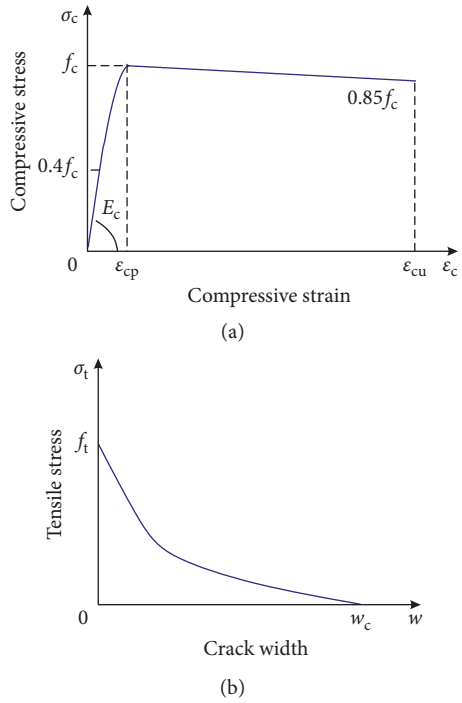

Figure 5: Material modelling of concrete. (a) Compression. (b) Tension.

where σ_c is the compressive stress at any point (MPa); ε_c is the compressive strain at any point; E_c is Young's modulus (MPa); f_c is the compressive strength of concrete (MPa); k is the plasticity number, $k = E_c \cdot \varepsilon_{cp}/f_c$; η is the ratio of strain to peak strain, $\eta = \varepsilon_c/\varepsilon_{cp}$, $\varepsilon_{cp} = 0.002$; and $\varepsilon_{cu} = 13.6\ \varepsilon_{cp}$.

For uncracked concrete subjected to tension, a linear stress-strain relationship was adopted. As shown in Figure 5(b), for a cracked section, a nonlinear approach for the stress-crack width relationship can be determined by using the following equation, referring to the study of Hordijk [25]:

$$\frac{\sigma_t}{f_t} = \left[1 + \left(c_1 \cdot \frac{w}{w_c}\right)^3\right] \cdot \exp\left(-c_2 \cdot \frac{w}{w_c}\right) - \frac{w}{w_c} \cdot \left(1 + c_1^3\right) \cdot \exp\left(-c_2\right), \tag{2}$$

where σ_t is the tensile stress of concrete (MPa); f_t is the tensile strength (MPa); w is the crack width (mm); w_c is the crack width at the complete release of stress, $w_c = 5.14\ G_F/f_t$ (mm); G_F is the fracture energy required to create a unit area of stress-free crack, $G_F = 0.073\ f_c^{0.18}$ (N/mm); and the constants are $c_1 = 3$ and $c_2 = 6.93$.

The concrete damaged plasticity model was used to describe the degraded response of the concrete material. Two independent uniaxial damage variables, d_c and d_t, were adopted to depict the damage of concrete due to compressive crushing and tensile cracking [17].

For concrete in compression, the evolution of d_c is associated with the plastic strain ε_c^{pl}, which is determined proportional to the inelastic strain $\varepsilon_c^{in} = \varepsilon_c - \sigma_c/E_c$, using a constant factor b_c $(0 < b_c < 1)$ in the following equation as suggested by Birtel and Mark [26]:

$$d_c = 1 - \frac{\sigma_c}{E_c \cdot \varepsilon_c^{pl} \cdot \left(1/b_c - 1\right) + \sigma_c}, \tag{3}$$

where d_c is the concrete compressive damage component and b_c is the ratio of the plastic strain to inelastic strain, $b_c = \varepsilon_c^{pl}/\varepsilon_c^{in}$, and b_c is taken as 0.7 [26].

For concrete in tension, the damage evolution component d_t is related to the "plastic" crack width w^{pl}, which is

proportional to the crack width w, using a constant factor b_t ($0 < b_t < 1$) in the following equation, referring to [26]:

$$d_t = 1 - \frac{\sigma_t \cdot l_0}{E_c \cdot w^{pl} \cdot (1/b_t - 1) + \sigma_t \cdot l_0}, \quad (4)$$

where d_t is the tensile damage variable of concrete; l_0 is assumed to be the unit length; and b_t is the ratio of the "plastic" crack width to the crack width, $b_t = w^{pl}/w$, and b_t is set as 0.1 [26].

3.5. Material Modelling of Steel. As shown in Figure 6, the stress-strain relationship of structural and reinforcing steel was modelled by trilinear curves. The initial stage is assumed to be elastic with Young's modulus E_s, followed by a branch of yielding and finally a regime of strain hardening. The stress-strain relationships for steel in tension and compression were assumed to be the same.

The headed stud, especially the region around the stud root, experiences complex stress state and large deformation. To improve the accuracy of simulation, the material of the stud was modelled by a trilinear stress-strain curve, as shown in Figure 7. The material behavior of the stud is initially elastic with Young's modulus E_s followed by strain hardening and then yielding.

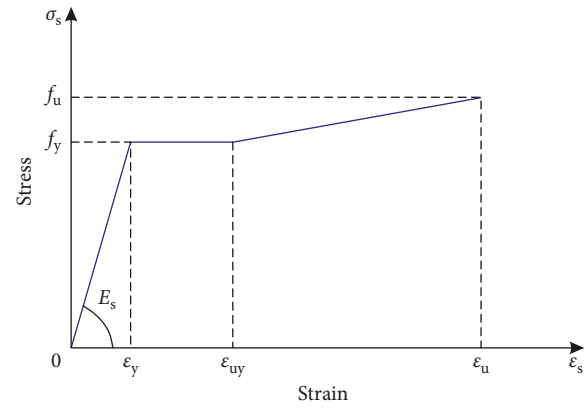

Figure 6: Material modelling of structural and reinforcing steel.

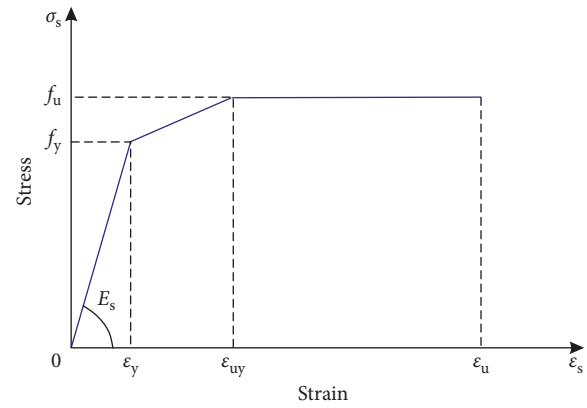

Figure 7: Material modelling of the headed stud.

4. Analysis Results and Verification

4.1. Failure Mode. As shown in Figure 8, the numerical results resembled the push-out failure of the headed stud, perfobond rib, and mixed shear connector quite well. The specimens with the headed stud failed due to stud shank fracture and concrete crushing below the stud root. The failure modes of the specimens with the perfobond rib were characterized by a crack in the concrete slab, yield of the perforating rebar, and shear failure of the concrete dowel. The push-out failure of the mixed shear connector was caused by the stud shank fracture, concrete crushing below the stud root, yield of the perforating rebar, and concrete dowel shear at the same time.

4.2. Local Response Stress. Figure 9 shows the local response stress of headed studs, perfobond ribs, and mixed shear connectors at the specimen failure. It was indicated that the mixed shear connectors had distributions of Mises stress in the stud shank similar to those of headed studs, and distributions of shear stress in the concrete dowel were similar to those of perfobond ribs. As shown in Figures 9(a) and 9(c), the Mises stress at the top and bottom of the stud shank decreased with the increase of distance to the stud root. The maximum Mises stress occurred near the stud root and exceeded the ultimate strength of headed studs that equaled 465 MPa, which revealed that the headed studs were shorn off at this region. As shown in Figures 9(b) and 9(d), the shear stress on the left and right of the concrete dowel increased until reaching about 2/3 of the distance to the bottom and then gradually decreased to zero at the top. It was shown that the shear stress in most part of the concrete dowel exceeded the allowable shear strength of concrete, which indicated dowel shear failures of perfobond ribs and mixed shear connector. The analysis results of local response stress agreed with the material behaviors of steel and concrete and thus further validated the reliability of the finite element method.

4.3. Load-Slip Behavior. As listed in Table 2, the accuracy of the proposed finite element model can be verified by comparison with push-out test results. The load-slip curves obtained from the finite element analysis were in good agreement with those of the experimental results, as shown in Figure 10. For specimens with the headed stud, the analyzed shear strength accounted for 94% to 96% of the experimental results. For specimens with the perfobond rib, the analyzed shear strength took up 99% to 105% of the mean test result. And the analyzed shear strength of the specimen with the mixed shear connector was among 90% to 104% of the averaged test shear capacity. The shear strength and the corresponding peak slip from the push-out tests were successfully captured in the finite element analysis. However, the analyzed load-slip curves showed smaller stiffness than those obtained from the push-out tests at the initial loading stage. The reason might be that the accurate

(a)

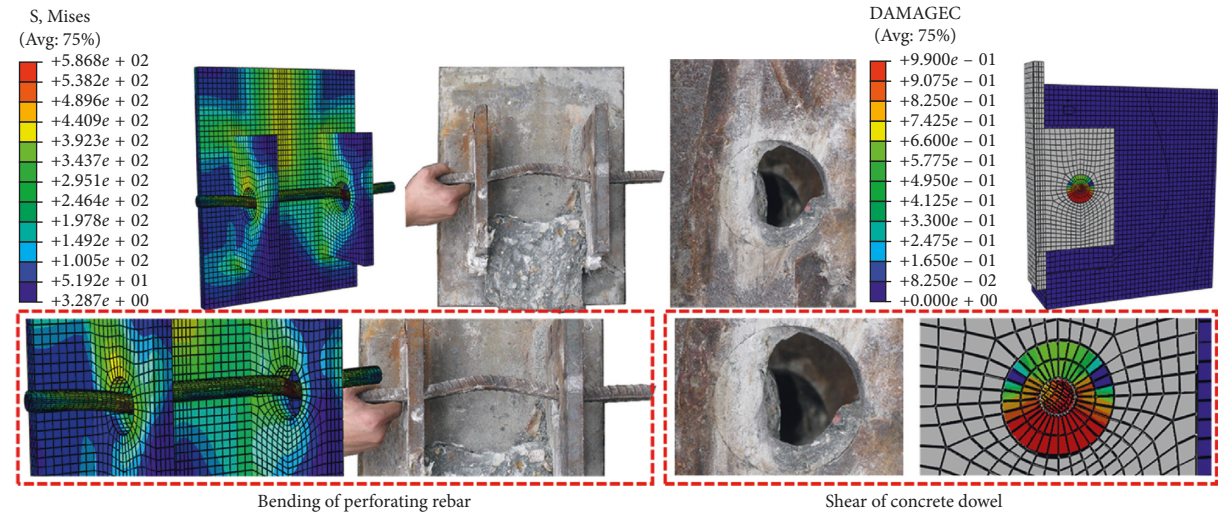

(b)

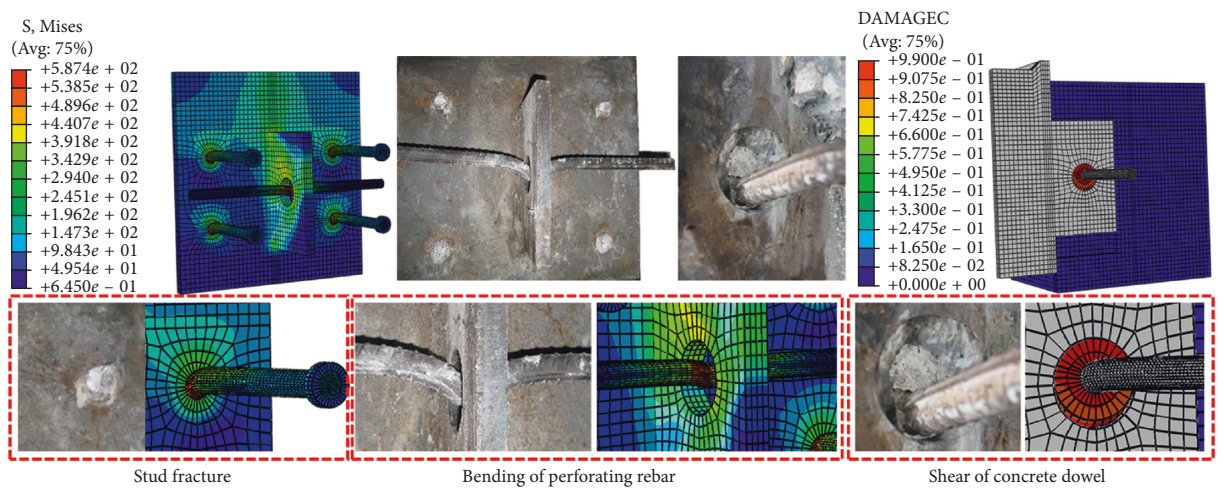

(c)

Figure 8: Tested and analyzed failure mode. (a) Headed stud. (b) Perfobond rib. (c) Mixed shear connector.

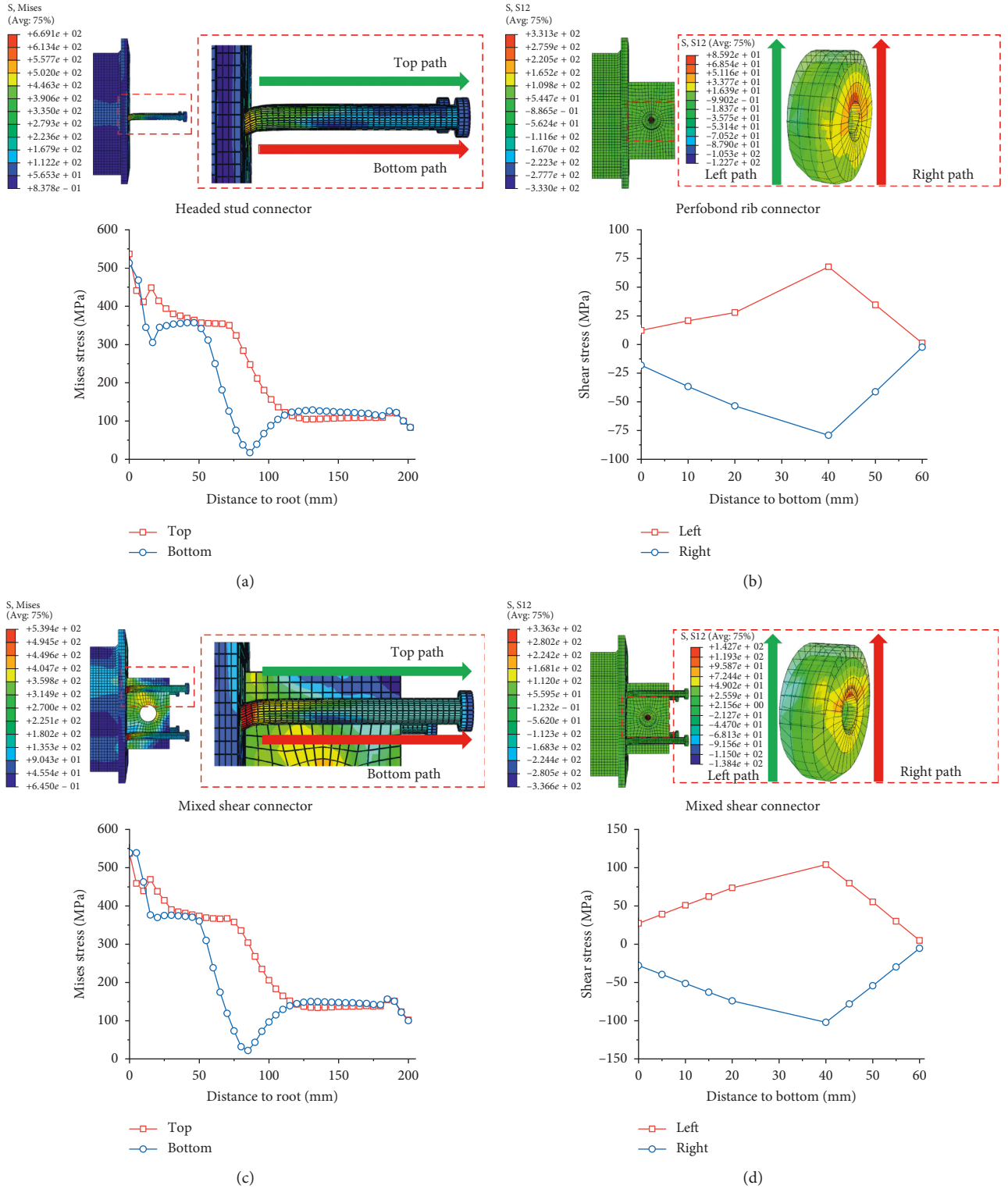

FIGURE 9: Local response stress. (a) Mises stress of the headed stud (HS). (b) Shear stress of the concrete dowel (PR). (c) Mises stress of the headed stud (MS). (d) Shear stress of the concrete dowel (MS).

friction and bonding effects between steel and concrete were difficult to simulate in the numerical models. Since the peak values and general patterns of the load-slip curves have been effectively resembled, the finite element model could be used to reveal the failure mechanism and generate reasonable parametric results.

Table 2: Comparison of analyzed and tested push-out results.

Specimen	Tested shear capacity		Analyzed shear capacity	Comparison	
	$V_{u,i}$ (kN)	$V_{u,avg}$ (kN)	$V_{u,fea}$ (kN)	$V_{u,fea}/V_{u,i}$	$V_{u,fea}/V_{u,avg}$
HS-1	—			—	
HS-2	233.9	236.5	224.2	0.96	0.95
HS-3	239.0			0.94	
PR-1	438.5			0.99	
PR-2	420.0	424.0	436.4	1.04	1.03
PR-3	413.5			1.05	
MS-1	1257.3			0.93	
MS-2	1128.2	1230.6	1175.1	1.04	0.95
MS-3	1306.3			0.90	

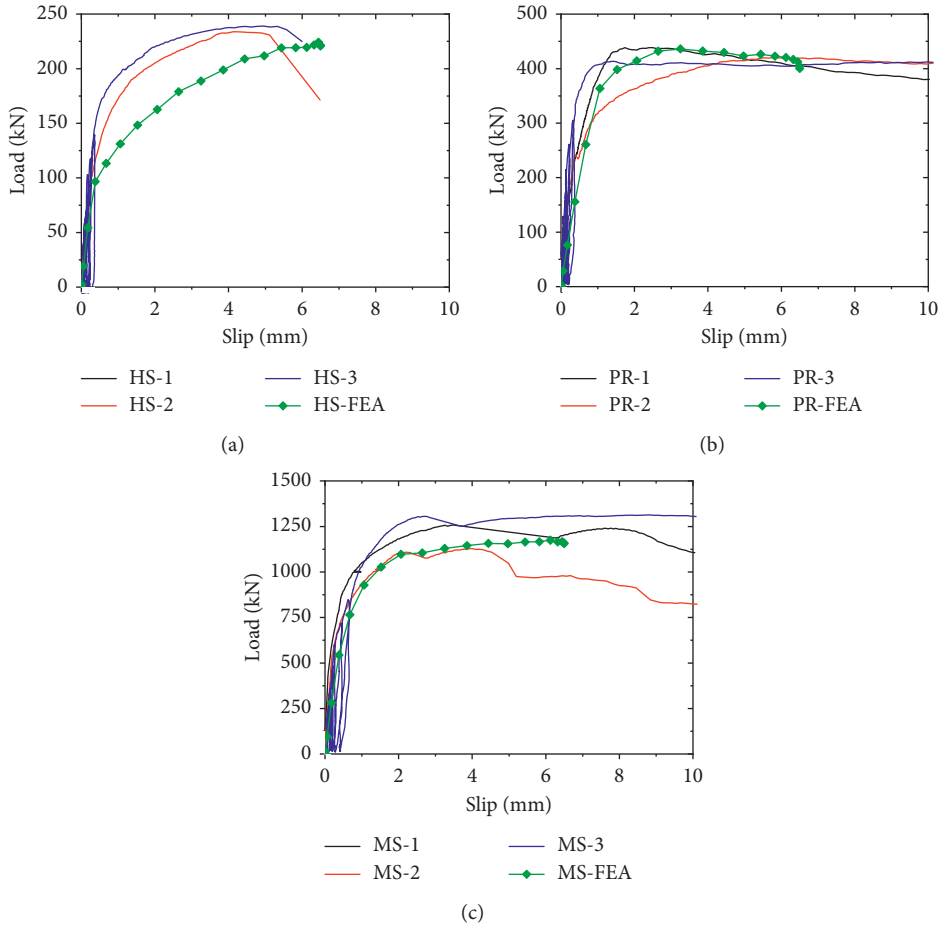

Figure 10: Comparison of analyzed and tested load-slip curves. (a) Headed stud. (b) Perfobond rib. (c) Mixed shear connector.

5. Parametric Study

Based on the validated finite element model, a total of 19 push-out tests were simulated to study the effects of connector dimension and material properties, as shown Table 3. The investigated variables included the stud diameter, hole diameter, rebar diameter, stud strength, concrete strength, and rebar strength. The connector dimension and material properties of models SD-22, SS-N, HD-60, RD-20, RS-N, and CS-70 were identical to those of the reference model RF. The shank diameter of all the models was 200 mm. The yield strength and tensile strength of steel beam were kept constant as 410 MPa and 545 MPa, respectively.

5.1. Effect of Stud Diameter. Figure 11 shows the effect of the stud shank diameter on the load-slip behavior of the mixed shear connector. When the stud shank diameter was added from 16 mm to 19 mm, 22 mm, 25 mm, and 30 mm, the shear capacity increased by 10%, 22%, 32%, and 53%, respectively. It was indicated that the increase of the stud shank diameter would lead to great increase of the shear capacity of the mixed shear connector. The mixed

Table 3: Generalization of parametric models.

Model	Headed stud			Perfobond rib				Concrete	Shear capacity
	d_s (mm)	f_{sy} (MPa)	f_{su} (MPa)	d_p (mm)	d_r (mm)	f_{ry} (MPa)	f_{ru} (MPa)	f_{cu} (MPa)	V_u (kN)
RF	22	370	465	60	20	382	547	70	1175.1
SD-16	16	370	465	60	20	382	547	70	964.4
SD-19	19	370	465	60	20	382	547	70	1062.3
SD-22	22	370	465	60	20	382	547	70	1175.1
SD-25	25	370	465	60	20	382	547	70	1270.0
SD-30	30	370	465	60	20	382	547	70	1478.0
SS-N	22	370	465	60	20	382	547	70	1175.1
SS-H	22	650	675	60	20	382	547	70	1291.3
HD-40	22	370	465	40	20	382	547	70	1078.0
HD-50	22	370	465	50	20	382	547	70	1117.5
HD-60	22	370	465	60	20	382	547	70	1175.1
HD-70	22	370	465	70	20	382	547	70	1224.1
HD-80	22	370	465	80	20	382	547	70	1340.5
RD-16	22	370	465	60	16	382	547	70	1088.3
RD-18	22	370	465	60	18	382	547	70	1151.8
RD-20	22	370	465	60	20	382	547	70	1175.1
RD-22	22	370	465	60	22	382	547	70	1216.9
RD-25	22	370	465	60	25	382	547	70	1252.6
RS-N	22	370	465	60	20	382	547	70	1175.1
RS-H	22	370	465	60	20	480	623	70	1213.0
CS-30	22	370	465	60	20	382	547	30	750.7
CS-40	22	370	465	60	20	382	547	40	889.0
CS-50	22	370	465	60	20	382	547	50	978.9
CS-60	22	370	465	60	20	382	547	60	1081.1
CS-70	22	370	465	60	20	382	547	70	1175.1

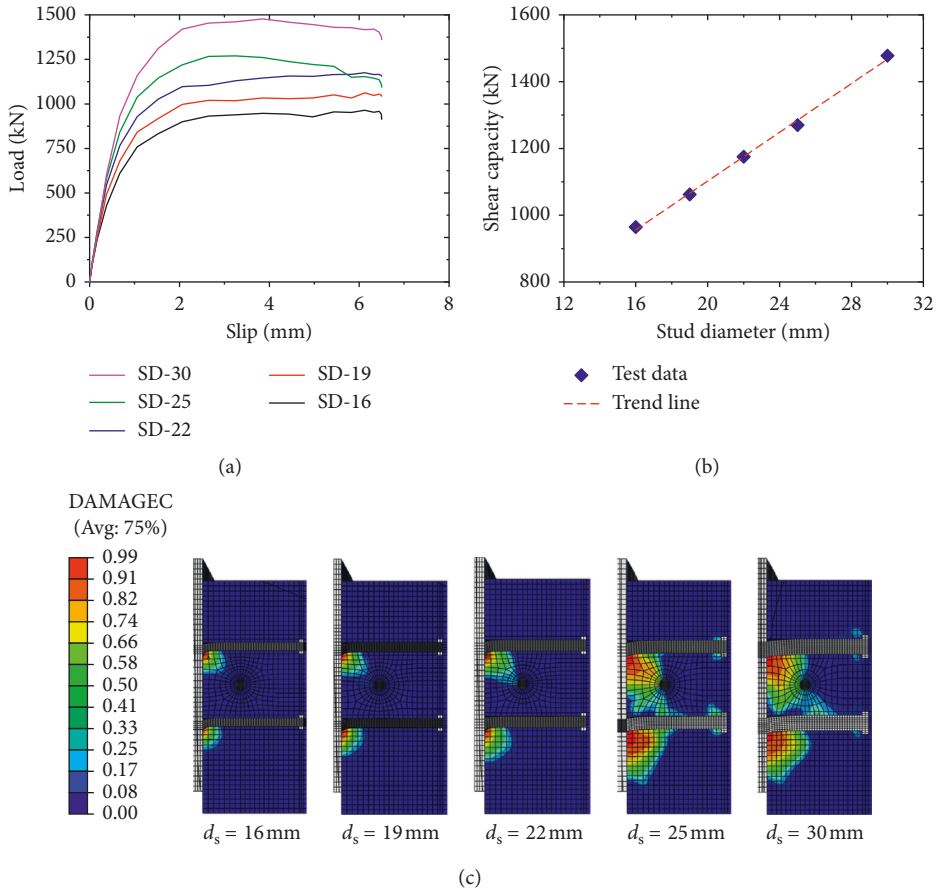

Figure 11: Effect of stud diameter. (a) Load-slip curves. (b) Influence analysis. (c) Failure mode.

shear connector failed due to stud fracture, concrete crushing at the stud root, and shear of the concrete dowel. As the larger stud was used, a larger region of the concrete below the stud root was involved in resisting the shear load.

5.2. Effect of Stud Strength. Figure 12 shows the effect of the stud strength on the load-slip behavior of mixed shear connector. When the headed stud's yield strength was increased from 370 MPa to 650 MPa, the shear capacity of the mixed shear connector increased by 10%. It was indicated that increasing the stud strength would lead to little increase in the shear capacity of the mixed shear connector. The analyzed failure mode of the mixed shear connector was still stud fracture, concrete crushing at the stud root, bending deformation of the perforating rebar, and shear of the concrete dowel. As the high strength stud was used, a larger region of the concrete below the stud root damaged before the connector failure.

5.3. Effect of Hole Diameter. Figure 13 shows the effect of the perfobond rib's hole diameter on the load-slip behavior of mixed shear connector. When the hole diameter was added from 40 mm to 50 mm, 60 mm, 70 mm, and 80 mm, the shear capacity increased by 4%, 9%, 14%, and 24%, respectively. It was indicated that the increase of the perfobond rib's hole diameter would lead to increase of the shear capacity of the mixed shear connector. As the larger hole was used for the perfobond rib, more concrete near the concrete dowel would be involved in resisting the shear load.

5.4. Effect of Rebar Diameter. Figure 14 shows the effect of the perforating rebar's diameter on the load-slip behavior of mixed shear connector. When the rebar diameter was added from 16 mm to 18 mm, 20 mm, 22 mm, and 25 mm, the shear capacity increased by 6%, 8%, 12% and 15%, respectively. It was indicated that the increase of the rebar diameter would lead to increase of the shear capacity of the mixed shear connector. The failure mode of the mixed shear connector was characterized by the stud fracture, concrete crushing, shear of the concrete dowel, and bending of the perforating rebar in hole. As the larger rebar was used, a larger region of the concrete near the concrete dowel was involved in resisting the shear load, and less bending deformation was observed for the perforating rebar.

5.5. Effect of Rebar Strength. Figure 15 shows the effect of the rebar strength on the load-slip behavior of mixed shear connector. When the perforating rebar's yield strength was increased from 382 MPa to 480 MPa, the shear capacity of the mixed shear connector increased by 3%. It was revealed that increasing the rebar strength would lead to little increase in the shear capacity of the mixed shear connector. The analyzed failure modes of the mixed shear connector included stud fracture, concrete crushing, shear of the concrete dowel, and bending of the perforating rebar in hole. Similar failure modes were observed for the finite element models using normal strength and high strength rebars.

5.6. Effect of Concrete Strength. Figure 16 shows the effect of the concrete strength on the load-slip behavior of the mixed shear connector. When the concrete strength was added from 30 MPa to 40 MPa, 50 MPa, 60 MPa, and 70 MPa, the shear capacity increased by 18%, 30%, 44%, and 57%, respectively. It was indicated that the increase of the concrete strength would lead to great increase of the shear capacity of the mixed shear connector. As the higher strength concrete was used, smaller region of the damaged concrete below the concrete dowel was observed in the analyzed failure modes.

6. Shear Capacity Equation

6.1. Existing Equation for Headed Stud. Eurocode 4 [27] provides the following design equation for specifying the shear capacity of the headed stud installed by automatic welding:

$$V_{su} = \frac{0.29\alpha d_s^2 \sqrt{E_c f_c}}{\gamma_V} \leq \frac{0.8 f_{su}\left(\pi d_s^2/4\right)}{\gamma_V}, \tag{5}$$

where V_{su} is the shear capacity per stud (N); d_s is the diameter of the shank of the headed stud (mm); E_c is the elastic modulus of concrete (MPa); f_c is the concrete compressive strength (MPa); f_{su} is the ultimate tensile strength of the headed stud but not greater than 500 MPa; γ_V is the partial factor (=1.25); and $\alpha = 0.2(l_s/d_s + 1)$ for $3 \leq l_s/d_s \leq 4$ and $\alpha = 1$ for $l_s/d_s > 4$.

AASHTO LRFD [28] specifies the nominal shear capacity of the headed stud embedded in concrete as equation follows:

$$V_{su} = 0.5\varphi A_s \sqrt{E_c f_c} \leq \varphi f_{su} A_s, \tag{6}$$

where A_s is the cross-sectional area of the shank of headed stud (mm^2) and φ is the resistance factor (=0.85).

The Chinese standard for design of steel structures (GB 50017-2017) [29] evaluates the shear capacity of headed stud by using the following equation:

$$V_{su} = 0.43 A_s \sqrt{E_c f_c} \leq 0.7 f_{su} A_s. \tag{7}$$

6.2. Existing Equation for Perfobond Rib. The standard specifications for hybrid structures of JSCE [30] suggest the following design equation for predicting the shear capacity per hole of the perfobond rib with the perforating rebar:

$$V_{pu} = \frac{1}{\gamma_b}\left\{1.85\left[\frac{\pi}{4}\left(d_p^2 - d_r^2\right) f_c + \frac{\pi}{4} d_r^2 f_{ru}\right] - 26.1 \times 10^3\right\}, \tag{8}$$

where V_{pu} is the shear capacity per stud (N); γ_b is the material coefficient (=1.3); d_p is the hole diameter (mm); d_r is the diameter of the rebar in hole (mm); and f_{ru} is the ultimate tensile strength of the rebar (MPa).

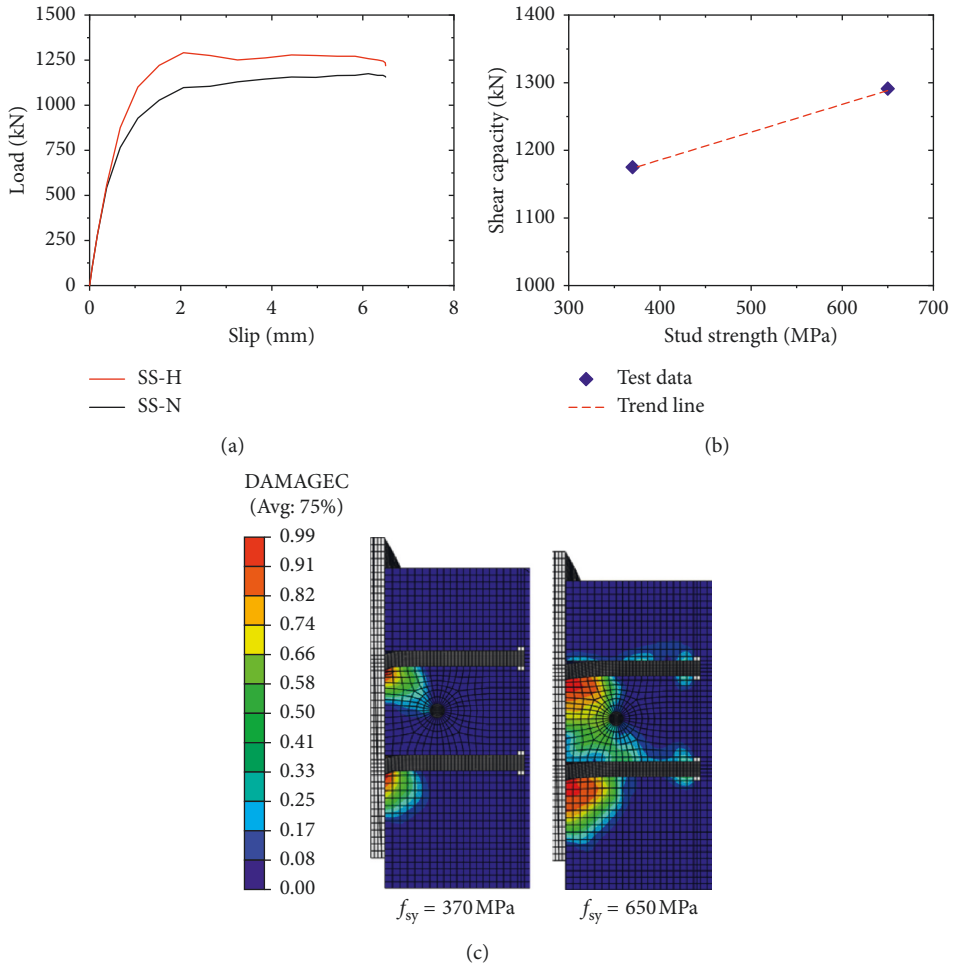

Figure 12: Effect of stud strength. (a) Load-slip curves. (b) Influence analysis. (c) Failure mode.

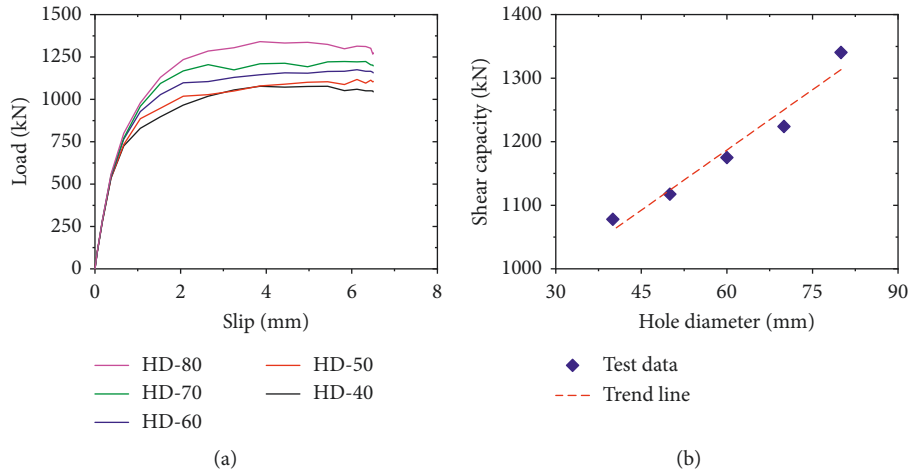

Figure 13: Continued.

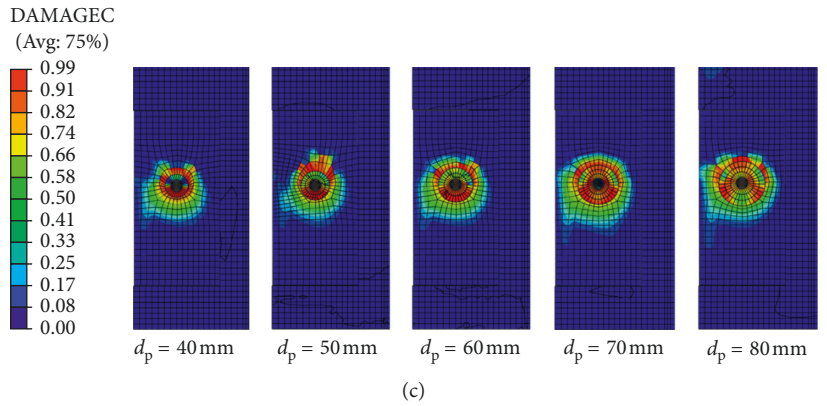

Figure 13: Effect of hole diameter. (a) Load-slip curves. (b) Influence analysis. (c) Failure mode.

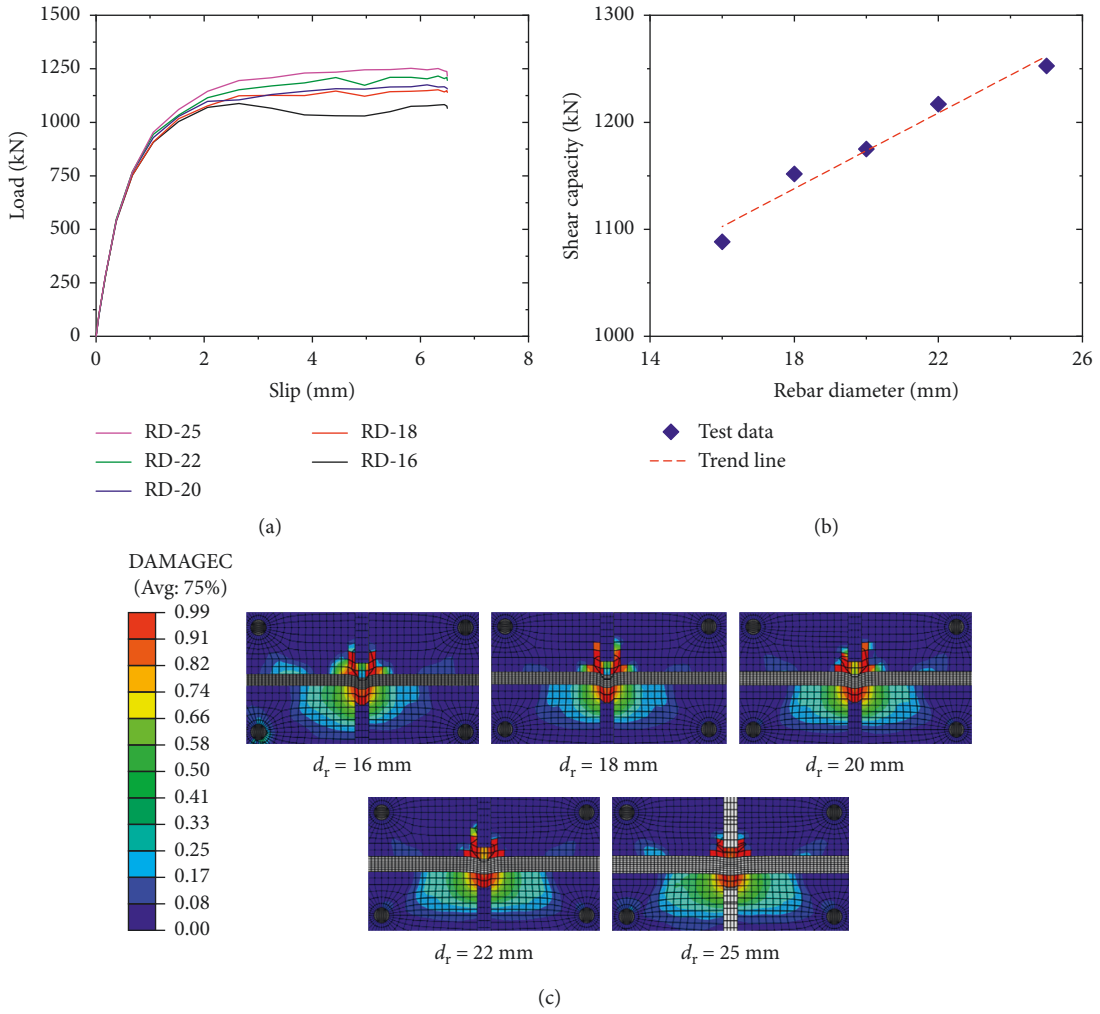

Figure 14: Effect of rebar diameter. (a) Load-slip curves. (b) Influence analysis. (c) Failure mode.

The Chinese specifications for design of highway steel bridge (JTG D64-2015) [31] evaluates the shear capacity per hole of the perfobond rib connector by using the following equation:

$$V_{pu} = 1.4\left(d_p^2 - d_r^2\right)f_c + 1.2d_r^2 f_{ry}, \quad (9)$$

where f_{ry} is the yield strength of the rebar (MPa).

6.3. Proposal for Mixed Shear Connector. According to the experimental and numerical results, the perfobond rib with headed stud mixed shear connector failed due to concrete crushing below stud root, stud shank fracture, shear of the concrete dowel, and bending of the perforating rebar. Referring to the existing shear capacity equations for the headed stud and perfobond rib, the contributions of these four items

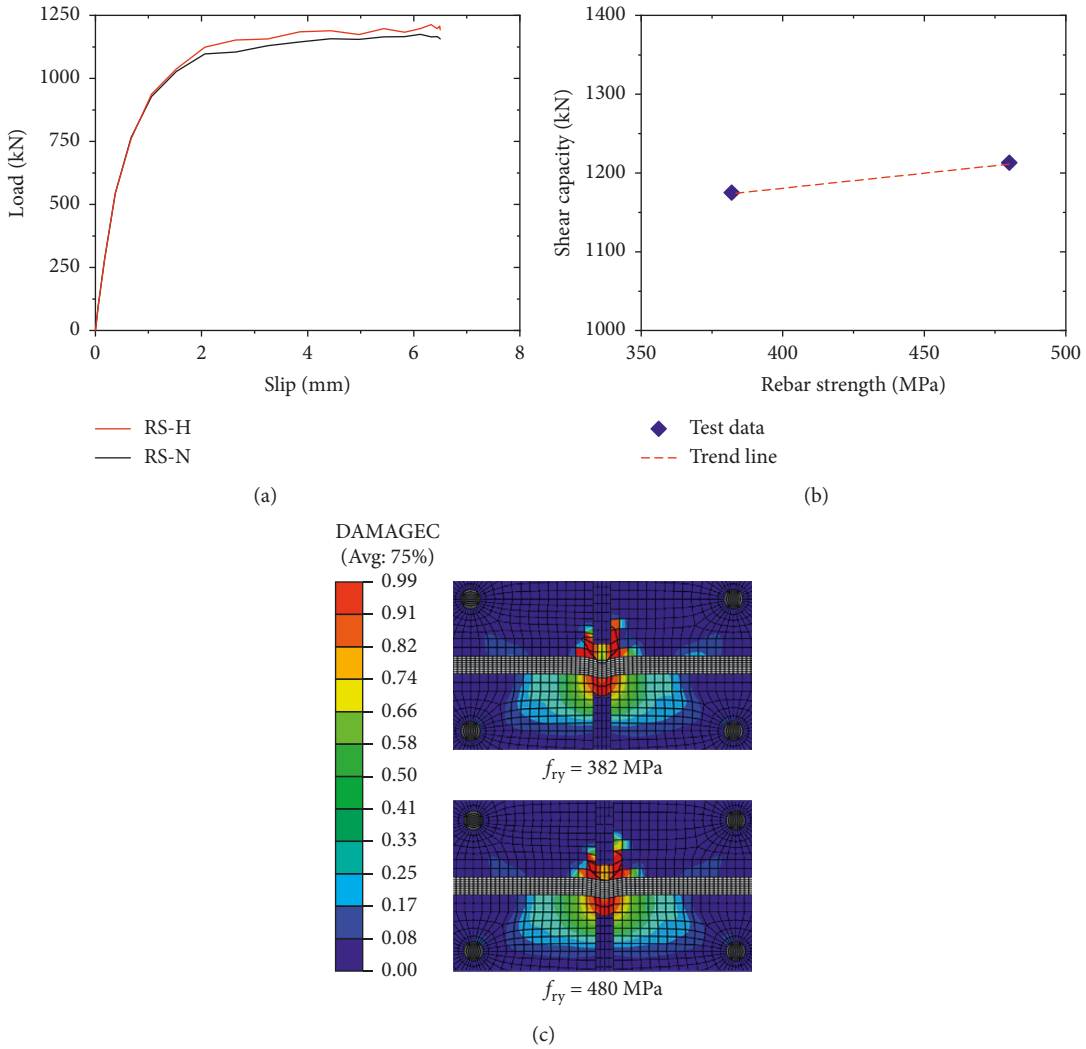

Figure 15: Effect of rebar strength. (a) Load-slip curves. (b) Influence analysis. (c) Failure mode.

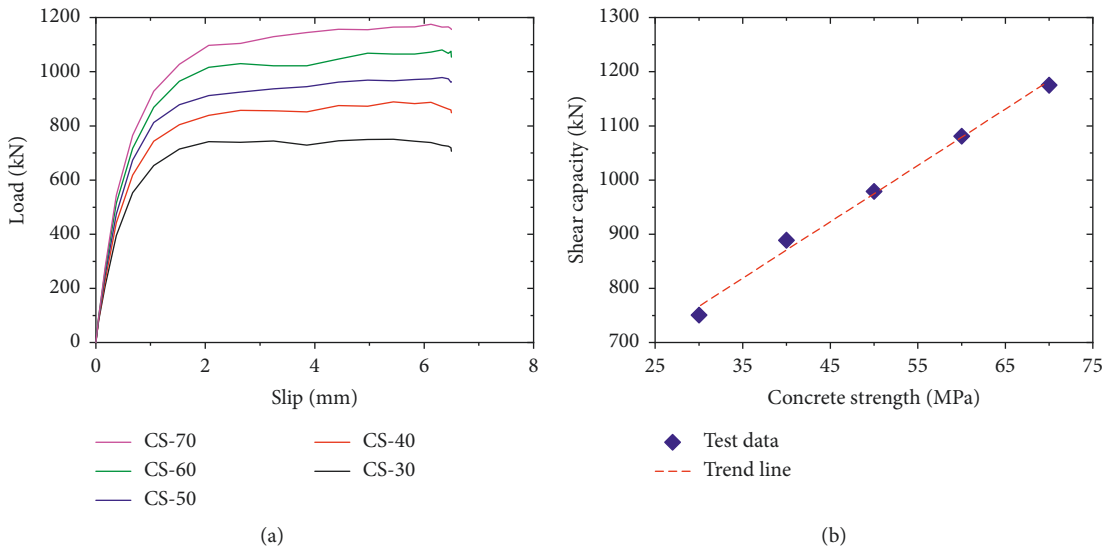

Figure 16: Continued.

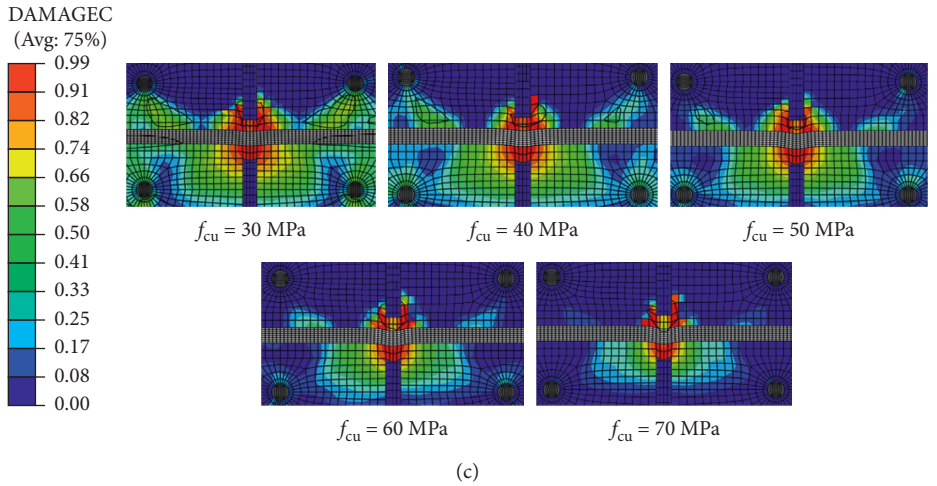

(c)

Figure 16: Effect of concrete strength. (a) Load-slip curves. (b) Influence analysis. (c) Failure mode.

Table 4: Comparison and validation of the proposed shear capacity equation.

Specimen	n_s	d_s (mm)	f_{cu} (MPa)	f_{su} (MPa)	n_p	d_p (mm)	d_r (mm)	f_{ry} (MPa)	V_u (kN)	$V_{u,eq}$ (kN)	$V_{u,eq}$ (V_u)
RF	4	22	70	465	1	60	20	382	1175.1	1171.6	1.00
SD-16	4	16	70	465	1	60	20	382	964.4	961.3	1.00
SD-19	4	19	70	465	1	60	20	382	1062.3	1058.1	1.00
SD-25	4	25	70	465	1	60	20	382	1270.0	1301.6	1.02
SD-30	4	30	70	465	1	60	20	382	1478.0	1555.3	1.05
SS-H	4	22	70	675	1	60	20	382	1291.3	1171.6	0.91
HD-40	4	22	70	465	1	40	20	382	1078.0	947.6	0.88
HD-50	4	22	70	465	1	50	20	382	1117.5	1048.4	0.94
HD-70	4	22	70	465	1	70	20	382	1224.1	1317.2	1.08
HD-80	4	22	70	465	1	80	20	382	1340.5	1485.2	1.11
RD-16	4	22	70	465	1	60	16	382	1088.3	1055.7	0.97
RD-18	4	22	70	465	1	60	18	382	1151.8	1110.4	0.96
RD-22	4	22	70	465	1	60	22	382	1216.9	1239.2	1.02
RD-25	4	22	70	465	1	60	25	382	1252.6	1352.7	1.08
RS-H	4	22	70	465	1	60	20	480	1213.0	1265.7	1.04
CS-30	4	22	30	465	1	60	20	382	750.7	782.2	1.04
CS-40	4	22	40	465	1	60	20	382	889.0	887.9	1.00
CS-50	4	22	50	465	1	60	20	382	978.9	986.9	1.01
CS-60	4	22	60	465	1	60	20	382	1081.1	1081.1	1.00
MS-1	4	22	70.3	465	1	60	20	382	1257.3	1174.2	0.93
MS-2	4	22	70.3	465	1	60	20	382	1128.2	1174.2	1.04
MS-3	4	22	70.3	465	1	60	20	382	1306.3	1174.2	0.90
SP-28-16-1	6	16	83.6	400	2	60	28	335	2318.5	2407.0	1.04
SP-28-16-2	6	16	83.6	400	2	60	28	335	2375.5	2407.0	1.01
SP-28-19-1	6	19	83.6	400	2	60	28	335	2581.5	2568.2	0.99
SP-28-19-2	6	19	83.6	400	2	60	28	335	2617.5	2568.2	0.98
SP-28-22-1	6	22	83.6	400	2	60	28	335	2953.0	2757.1	0.93
SP-28-22-2	6	22	83.6	400	2	60	28	335	2617.0	2757.1	1.05
SP-25-16-1	6	16	83.6	400	2	60	25	335	2123.5	2193.9	1.03
SP-25-16-2	6	16	83.6	400	2	60	25	335	2154.0	2193.9	1.02
SP-20-16-1	6	16	83.6	400	2	60	20	335	2019.5	1892.3	0.94
SP-20-16-2	6	16	83.6	400	2	60	20	335	1965.0	1892.3	0.96

could be evaluated by $d_s^2\sqrt{E_c f_c}$, $d_s^2 f_{su}$, $(d_p^2 - d_r^2) f_c$, and $d_r^2 f_{ry}$, respectively. Thus, an alternative equation combining these four contributions was proposed to evaluate the shear capacity of the mixed shear connector as follows:

$$V_{mu} = n_s\left(C_1 d_s^2\sqrt{E_c f_c} + C_2 d_s^2 f_{su}\right) + n_p\left[C_3\left(d_p^2 - d_r^2\right) f_c + C_4 d_r^2 f_{ry}\right], \tag{10}$$

where V_{mu} is the shear capacity per flange of mixed shear capacity (N); n_s is the number of headed studs per flange; n_p is the number of holes of the perfobond rib per flange; d_s is the stud shank diameter (mm); E_c is the elastic modulus of concrete (MPa); f_c is the concrete compressive strength (MPa); f_{su} is the ultimate tensile strength of the stud; d_p is the hole diameter (mm); d_r is the rebar diameter (mm); f_{ry} is the yield strength of the rebar (MPa); and C_1, C_2, C_3, and C_4 are coefficients.

Based on the nonlinear regression analysis on a total of 32 experimental and numerical results both in reference [32] and in this study, the best fitting of the coefficients in equation (10) could be derived as $C_1 = 0.16$, $C_2 = 0$, $C_3 = 2.0$, and $C_4 = 2.4$. Therefore, the final proposal for estimating the shear capacity of mixed shear connector could be given as follows:

$$V_{mu} = 0.16 n_s d_s^2 \sqrt{E_c f_c} + 2.0 n_p \left(d_p^2 - d_r^2\right) f_c + 2.4 n_p d_r^2 f_{ry}. \quad (11)$$

Table 4 presents the calculated shear capacities from (11), which were compared to the experimental and numerical results. The mean and variance of the ratio of predicted shear strengths to experimental results were 0.998 and 0.055, respectively. It was indicated that the predicted values agreed reasonably well with the results from push-out tests and parametric study, as shown in Figure 17. Therefore, (11) could be used to predict the shear capacity of the perfobond rib with the headed stud mixed shear connector in steel and concrete composite structures. The validity and accuracy of the model cannot be demonstrated on the basis of the reduced number of experimental data, and it is however limited within the range of parameter variation investigated.

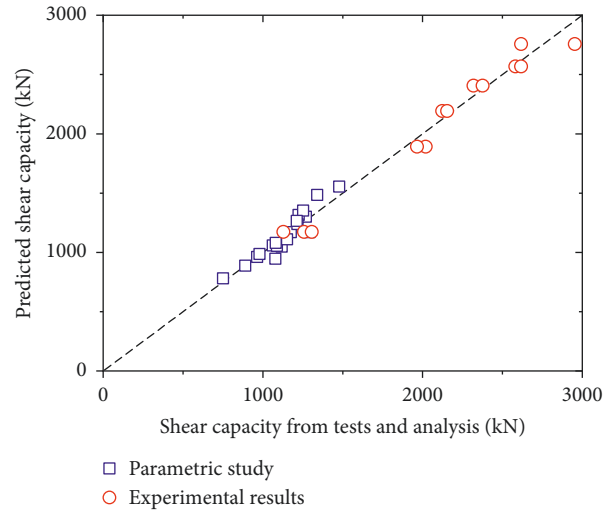

Figure 17: Comparison and validation of the proposed shear capacity equation.

7. Conclusions

In this study, nine push-out tests of the perfobond rib with the headed stud mixed shear connector were carried out. Based on the experimental results, parametric study, and analytical analysis, the following conclusions are drawn:

(1) The push-out failure modes of the perfobond rib with the headed stud mixed shear connector are characterized by the stud shank fracture, concrete crushing below the stud root, yield of the perforating rebar, and concrete dowel shear at the same time.

(2) The proposed finite element model is verified by comparison with push-out test results. The load-slip curves obtained from finite element analysis are in good agreement with experimental results.

(3) Based on the validated finite element model, a total of 19 push-out tests are simulated to study the effects of connector dimension and material properties. The shear capacity of the mixed shear connector increases with the increase of the stud diameter, rebar diameter, hole diameter, stud strength, rebar strength, and concrete strength.

(4) An analytical model is proposed to evaluate the shear capacity of the perfobond rib with the headed stud mixed shear connector. This proposal is validated by comparison with the parametric and experimental results.

The overall investigation may provide reference for the design and construction of shear connectors in steel and concrete composite structures.

Data Availability

The data used to support the findings of this study are available from the corresponding author upon request.

Conflicts of Interest

The authors declare that they have no conflicts of interest.

Acknowledgments

The research described in this paper was financially supported by the grants from the Natural Science Foundation of China (51808235), Fujian Provincial Natural Science Foundation of China (2018J05083), and Huaqiao University Scientific Research Funding (16BS804).

References

[1] F.-x. Ding, G.-a. Yin, H.-b. Wang, L. Wang, and Q. Guo, "Static behavior of stud connectors in bi-direction push-off tests," *Thin-Walled Structures*, vol. 120, pp. 307–318, 2017.

[2] S. Zheng, C. Zhao, and Y. Liu, "Experimental shear strength evaluation of perfobond shear connector with various hole shapes," *Structural Engineering and Mechanics*, vol. 67, no. 2, pp. 131–142, 2018.

[3] S.-H. Kim, S. Park, K.-S. Kim, and C.-Y. Jung, "Generalized formulation for shear resistance on Y-type perfobond rib shear connectors," *Journal of Constructional Steel Research*, vol. 128, pp. 245–260, 2017.

[4] C. H. Chung, J. Lee, and J. S. Kim, "Shear strength of T-type perfobond rib shear connectors," *KSCE Journal of Civil Engineering*, vol. 20, no. 5, pp. 1824–1834, 2016.

[5] M. Shariati, N. H. Ramli Sulong, and M. M. Arabnejad Khanouki, "Experimental assessment of channel shear connectors under monotonic and fully reversed cyclic loading in high strength concrete," *Materials & Design*, vol. 34, no. 2, pp. 325–331, 2012.

[6] X. Liu, M. A. Bradford, Q.-J. Chen, and H. Ban, "Finite element modelling of steel-concrete composite beams with high-strength friction-grip bolt shear connectors," *Finite Elements in Analysis and Design*, vol. 108, pp. 54–65, 2016.

[7] M. Classen and J. Hegger, "Assessing the pry-out resistance of open rib shear connectors in cracked concrete - engineering model with aggregate interlock," *Engineering Structures*, vol. 148, pp. 254–262, 2017.

[8] N. Gattesco, E. Giuriani, and A. Gubana, "Low-cycle fatigue test on stud shear connectors," *Journal of Structural Engineering*, vol. 123, no. 2, pp. 145–150, 1997.

[9] C. Xu, Q. Su, and H. Masuya, "Static and fatigue behavior of the stud shear connector in lightweight concrete," *International Journal of Steel Structures*, vol. 18, no. 2, pp. 569–581, 2018.

[10] H.-Y. Kim and Y.-J. Jeong, "Experimental investigation on behaviour of steel-concrete composite bridge decks with perfobond ribs," *Journal of Constructional Steel Research*, vol. 62, no. 5, pp. 463–471, 2006.

[11] J. He, Y. Liu, A. Chen, D. Wang, and T. Yoda, "Bending behavior of concrete-encased composite I-girder with corrugated steel web," *Thin-Walled Structures*, vol. 74, no. 9, pp. 70–84, 2014.

[12] Z. Lin, Y. Liu, and C. W. Roeder, "Behavior of stud connections between concrete slabs and steel girders under transverse bending moment," *Engineering Structures*, vol. 117, pp. 130–144, 2016.

[13] W. Xue, M. Ding, H. Wang, and Z. Luo, "Static behavior and theoretical model of stud shear connectors," *Journal of Bridge Engineering*, vol. 13, no. 6, pp. 623–634, 2008.

[14] S. Zheng, Y. Liu, T. Yoda, and W. Lin, "Shear behavior and analytical model of perfobond connectors," *Steel and Composite Structures*, vol. 20, no. 1, pp. 71–89, 2016.

[15] T. Hosaka, K. Mitsuki, H. Hiragi, Y. Ushijima, Y. Tachibana, and H. Watanabe, "An experimental study on shear characteristics of perfobond strip and its rational strength equations," *Journal of Structural Engineering-JSCE*, vol. 46A, pp. 1593–1604, 2000, in Japanese.

[16] E. C. Oguejiofor and M. U. Hosain, "Numerical analysis of push-out specimens with perfobond rib connectors," *Computers & Structures*, vol. 62, no. 4, pp. 617–624, 1997.

[17] ABAQUS, *ABAQUS Documentation, Version 6.10*, Dassault System, Boston, MA, USA, 2010.

[18] L. Ombres and S. Verre, *Shear Performance of FRCM Strengthened RC Beams*, ACI Special Publication, Farmington Hills, MI, USA, 2018.

[19] G. Fortunato, M. F. Funari, and P. Lonetti, "Survey and seismic vulnerability assessment of the baptistery of san Giovanni in Tumba (Italy)," *Journal of Cultural Heritage*, vol. 26, pp. 64–78, 2017.

[20] L. Ombres and S. Verre, "Masonry columns strengthened with steel fabric reinforced cementitious matrix (S-FRCM) jackets: experimental and numerical analysis," *Measurement*, vol. 127, pp. 238–245, 2018.

[21] S. Zheng, Y. Liu, T. Yoda, and W. Lin, "Parametric study on shear capacity of circular-hole and long-hole perfobond shear connector," *Journal of Constructional Steel Research*, vol. 117, pp. 64–80, 2016.

[22] S. Zheng, Y. Liu, Y. Liu, and C. Zhao, "Experimental and numerical study on shear resistance of notched perfobond shear connector," *Materials*, vol. 12, no. 3, p. 341, 2019.

[23] FIB, *Model Code 2010—Final Draft*, Vol. 1, FIB, Lausanne, Switzerland, 2010.

[24] H. T. Nguyen and S. E. Kim, "Finite element modeling of push-out tests for large stud shear connectors," *Journal of Constructional Steel Research*, vol. 65, no. 10-11, pp. 1909–1920, 2009.

[25] D. A. Hordijk, "Tensile and tensile fatigue behaviour of concrete; experiments, modelling and analyses," *Heron*, vol. 37, no. 1, pp. 3–79, 1992.

[26] V. Birtel and P. Mark, "Parameterised finite element modelling of RC beam shear failure," in *Proceedings of the 19th Annual International ABAQUS Users' Conference*, pp. 95–108, ABAQUS Inc, Boston, MA, USA, May 2006.

[27] EN 1994-1-1: 2004, *Eurocode 4: Design of Composite Steel and Concrete Structures, Part 1-1: General Rules and Rules for Buildings*, European Committee for Standardization (CEN), Brussels, Belgium, 2004.

[28] AASHTO, *AASHTO LFRD Bridge Design Specifications*, American Associate of State Highway and Transportation Officials, Washington, DC, USA, 4th edition, 2007.

[29] GB 50017-2017, *Code for Design of Steel Structures*, Ministry of Housing and Urban-rural Development of Peoples' Republic of China, Beijing, China, 2017, in Chinese.

[30] JSCE, *Standard Specifications for Hybrid Structures-2009*, Japan Society of Civil Engineers, Tokyo, Japan, 2009.

[31] JTG D64-2015, *Specifications for Design of Highway Steel Bridge*, Ministry of Transport of Peoples' Republic of China, Beijing, China, 2015, in Chinese.

[32] W. Deng, J. Zhang, D. Liu, J. Gu, J. Hu, and G. Huang, "Experimental behaviors and shear bearing capacity calculation of perfobond rib with head stud connectors," *Journal of Southeast University (Natural Science Edition)*, vol. 48, no. 3, pp. 463–469, 2018, in Chinese.